Topological classification for intersection singularities of exceptional surfaces in pseudo-Hermitian systems

Hongwei Jia[1,2,#], Ruo-Yang Zhang[1,#], Jing Hu[1], Yixin Xiao[1], Shuang Zhang[3], Yifei Zhu[4,*], C. T. Chan[1,†]

[1]Department of Physics, the Hong Kong University of Science and Technology, Clear Water Bay, Kowloon, Hong Kong, China

[2]Institute for Advanced Study, the Hong Kong University of Science and Technology, Clear Water Bay, Kowloon, Hong Kong, China

[3]Department of Physics, The University of Hong Kong, Pokfulam Road, Hong Kong 999007, China

[4]Department of Mathematics, Southern University of Science and Technology, Shenzhen, Guangdong, China

#These authors contributed equally to this work

Abstract: Non-Hermitian systems exhibit rich topological phenomena that are related to exceptional points. The exceptional points can form exceptional surfaces, which support embedded lower dimensional hypersurface singularities. In this study, we provide the first topological classification for degeneracy lines where exceptional surfaces intersect transversely, dubbed non-defective intersection lines, for a generic non-Hermitian system that has both parity-time and pseudo-Hermitian symmetries. By constructing the quotient space of order parameter space under equivalence relations of eigenstates, we reveal that the fundamental group of such gapless structures can be described by a non-Abelian free group on three generators. The classification predicts a new kind of non-Hermitian gapless topological phase featuring a chain of non-defective intersection lines in band structures. Furthermore, we predict the existence of topologically protected edge states in one-dimensional lattice models that originate from the intersection singularity. These edge states are unexpected for such gapless phases and cannot

be explained by the conventional Zak phase theory. Our work establishes a new framework for designing systems with robust topological phases based on exceptional surfaces and intersections and offers potential applications in sensing and lasing devices.

Introduction. Singularities are ubiquitous and play significant roles in various physical systems in the real world, often accompanied by exotic physical phenomena[1-13]. In topological materials, a Weyl point in a Hermitian system acts as a sink or source of the Berry curvature, and two Weyl points with opposite chiralities are connected by a Fermi-arc surface state[1,2,9,11]. The existence and stability of singularities can be better understood by topology, and a singularity can be characterized by a topological invariant, such as the Chern number. This invariant is usually encoded in the adiabatic evolution of eigenstates on closed loops/surfaces that enclose it[5,6-9,11]. Recently, the topology of non-Hermitian systems is attracting growing attention[14-25]. Exceptional points, unique features of non-Hermiticity, are singular points on the complex energy plane where both the eigenenergies and the eigenstates coalesce[14-19]. Exceptional points differ from degeneracies in Hermitian systems, such as Weyl/Dirac points and nodal lines, as they may carry fractional topological invariants[16,18,19,24,26], and can induce stable bulk Fermi-arcs[22,24] and braiding of eigenvalues[26]. The non-Hermitian skin effect, manifested by sensitivity of the eigen-spectrum to boundary conditions, is associated with the point gaps in bulk topology[15-18,21,23,25]. Recent discoveries of lines, rings and surfaces of exceptional points have further enriched the classes of topological degeneracies[27-31]. High-order exceptional degeneracies, which frequently appear as cusps of exceptional lines/surfaces, carry hybrid topological invariants in a higher dimensional parameter space[32].

Significant efforts have recently been devoted to classifying exceptional points. Topological classifications are particularly important, as they enable the prediction of degeneracies in the parameter space when the type of energy gaps and Altland-Zirnbauer symmetry class for the system are known.[14,19,20,33-35]. This provides a theoretical framework for predicting non-Hermitian topological phases of matter and guiding experimental realizations. Exceptional points, in particular, can assemble into hypersurfaces in 3D parameter space, dubbed exceptional surfaces (ESs), that separate exact and

broken phases[20]. ESs are commonly observed in non-Hermitian systems with parity-time inversion symmetry (PT) or chiral symmetry[20,27-29], and have broad applications in the design of sensing and absorption devices[31,36]. As a subspace of the parameter space, ESs may possess embedded lower-dimensional singularities, the so-called hypersurface singularities that have remarkable properties differentiating them from other points on the ESs, such as intersections[37], cusps[38-40], and swallowtail catastrophes[41]. Such hypersurface singularities are symmetry protected[31,37-41], and are stable against perturbations with symmetries preserved. However, despite various important physical phenomena and potential applications, the hypersurface singularities on ESs have not yet been topologically classified.

In this work, we provide the first topological classification for a typical hypersurface singularity where exceptional surfaces intersect transversely, which are dubbed non-defective intersection lines (NIL) of ESs, in two band models. NIL represents the simplest form of hypersurface singularities, and can be commonly found in a generic non-Hermitian systems with PT symmetry and an additional pseudo-Hermitian symmetry[41]. The band structures of such systems feature a gapless structure composed of ESs and the embedded NILs. We analyze equivalence relations of eigenstates and discover that the quotient space of the order-parameter space is homotopy equivalent to a bouquet of three circles $M = S^1 \vee S^1 \vee S^1$. The topology of the NIL is thus represented by the fundamental group of *M*, which is a non-Abelian free group on three generators. Importantly, we introduce intersection homotopy theory to classify such non-isolated singularities for the first time, which is very different from conventional homotopy theory that addresses isolated ones[6,26,32-35,40]. Exotic physical phenomena arising from the nontrivial topology of the NIL, such as the chain of NILs, can be systematically explained with our classification. In addition, the stable edge states in one-dimensional lattice models protected by the topological NIL, which is counter-intuitive for gapless phases and cannot be explained by the conventional Zak phase theory, can also be predicted with our topological description.

Main. The prototypical Hamiltonian is a two-level system, which is *PT* symmetric and also preserves an additional η-pseudo-Hermitian symmetry[41-43]

$$[H, PT] = 0, \qquad \eta H \eta^{-1} = H^{\dagger} \tag{1}$$

The *PT* operator can be regarded as complex conjugation with a proper choice of basis in parameter space, and thus the Hamiltonian can always be gauged to be real. The metric operator η here takes the Minkowski metric $\eta = \mathrm{diag}(-1,1)$ [13,41,44,45]. More details on pseudo-Hermiticity are provided in Section 1 of supplementary information. These symmetries imply that the **k**-space Hamiltonian can be written in the form

$$H(\mathbf{k}) = f_2(\mathbf{k}) i\sigma_2 + f_3(\mathbf{k})\sigma_3 \tag{2}$$

where $f_{2,3}$ are real functions of three-dimensional (3D) **k**-space, and $\sigma_{2,3}$ are Pauli matrices. The term multiplied by an identity matrix can be ignored because it has no impact on the gapless structure. Such Hamiltonians correspond to physical systems with non-reciprocal hopping[41,46-48] of orbitals.

The 2D f_2-f_3 plane serves as the order parameter space of all Hamiltonians that preserve the symmetries specified in Eq. (1). This is because any exceptional surfaces (ESs) in the 3D **k**-space correspond to exceptional lines (ELs) at $f_2 = \pm f_3$ on the 2D f_2-f_3 plane. At the lines where the ESs intersect transversely (i.e. the NILs) in the 3D **k**-space, which in turn correspond to the intersecting point (termed non-defective intersection point, NIP) of the ELs at the origin $f_2 = f_3 = 0$. Moreover, a path traced in the 3D **k**-space can be mapped to a path on the 2D f_2-f_3 plane, and if the path encircles around an NIL in the 3D **k**-space, the corresponding path on the 2D f_2-f_3 plane encircles around the NIP. The gapless structure of the order parameter space is shown in Fig. 1a, with the red and green lines representing different ELs satisfying $f_2 = \mp f_3$, respectively. Regions I and III (satisfying $|f_2| < |f_3|$) have real eigenenergies and are referred to as *PT*-exact phases. On the other hand, regions II and IV ($|f_2| > |f_3|$) are *PT*-broken phases, where the eigenvalues form complex-conjugate pairs. The paths α, α', β and β' are terminated at ELs, and are residing in different regions (Fig. 1a). The NIP at the origin is what we aim to classify, and is excluded from the 2D plane[20,49]. Thus, any paths or loops cannot traverse the NIP. First, the 2D plane with a hole at the origin can deformation retract to a circle S^1 (Fig. 1b). Such a mathematical process can be interpreted as a quotient map, which identifies all points on the ray starting from the origin (excluding the origin). The identification is based on an equivalence

relation that all points on the ray have the same eigenstates ordered by eigenvalues. Consequently, the upper and lower halves of EL_1 shrink to antipodal points A and A', respectively. A similar process applies to EL_2, with the upper and lower halves shrinking to B and B', respectively. There are also two equivalence relations on the S^1. At point A, the two eigenstates coalesce, which is the same as the coalesced eigenstate at point A'. Therefore, A and A' can be identified, and one can glue A' to A via a quotient map. The same procedure applies to B and B'. It is important to note that antipodal points locating in the regions that eigenenergies are gapped cannot be identified because their eigenstates are ordered inversely based on the eigenenergies. Using the above procedures, we obtain the quotient space (detailed mathematical discussions on quotient space are in Section 2 of supplementary information) of the S^1 in Fig. 1b, which is a bouquet of three circles (see Fig. 1c),

$$M = S^1 \vee S^1 \vee S^1 \tag{3}$$

The fundamental group of M can thus be derived

$$\pi_1(M) = \mathbf{Z} * \mathbf{Z} * \mathbf{Z} \tag{4}$$

being a free non-Abelian group on three generators. As shown in Fig. 1c, the three generators of the group Z_1, Z_2 and Z_3 can be described by the combinations of paths $\alpha\beta$, $\alpha\alpha'^{-1}$ and $\alpha'\beta'$, respectively. These topological invariants are associated with the frame deformations of eigenstates on these paths, which are explained in detail in Section 3 of supplementary information.

We next introduce loops (or combined paths) in parameter space that carry nontrivial and trivial topological invariants to better understand the group. The combined paths characterizing the generators Z_1, Z_2 and Z_3 are shown in Fig. 2a-c, respectively, where the dashed lines with arrows denote quotient maps that glue identified points. We note that the gluing process does not mean the loop traverses the NIP. Each of the combined paths corresponds to an S^1 in Fig. 1c, which are exactly closed loops in quotient space M. A closed loop encircling the NIP is also a path combination $\alpha\beta\alpha'\beta'$, which characterizes the topological invaraint Z_1Z_3, being an element in the group [Eq. (4)]. Some other nontrivial loops are discussed in Section 4 of supplementary information. Typical loops carrying a trivial topological invariant are shown in Fig. 2e-g. The loop l does not touch any EL, and thus is

confined in only one region, which is always trivial because it cannot enclose any singularity (i.e. the excluded point, NIP). As we move the loop across the EL, l is decomposed into two paths l_1 and l_2 (Fig. 2f). As the terminal points of l_1 (or l_2) can be identified, l_1 (or l_2) is also a loop in quotient space M, and is a trivial loop that can shrink to a point without encountering the NIP. Therefore, the combination $l_1 l_2$ is also trivial. By stretching the loop to cross the other EL (see Fig. 2g), l becomes a composite of $l_1 l_3 l_4 l_5$. Since both l_1 and l_4 correspond to trivial loops in quotient space M, the composite is equivalent to the combination $l_3 l_5$. In addition, paths l_3 and l_5 are along opposite directions and are homotopic to α^{-1} and α, respectively. It is thus not difficult to find out that the combination $l_1 l_3 l_4 l_5$ remains trivial. *From this analysis, we can conclude that a loop (or a path) encountering ELs through continuous deformations will not change the topology. In contrast, encountering NIPs is not allowed, which will change the topology.* Similar conclusions can also be found in Ref. 41. As an important point, a path joining ELs (or ESs) can provide a lot of information on the NIP (see more details in Section 4 of supplementary information) even though it appears open in the parameter space, which is substantially different from isolated singularities. Therefore, if a loop is partitioned into several segments by ELs (or ESs), it is necessary to investigate the evolution of eigenstates on each path and then discuss the combinations. Since the non-trivial loops all traverse the hypersurfaces, our method is affiliated to intersection homotopy theory[49,50].

We next aim to understand the formation of chain-like structures composed of NILs and their evolution as the Hamiltonian deforms based on our topological description. The chain of singular lines in parameter space is a nontrivial phenomenon that has previously been observed for nodal lines in PT-symmetric Hermitian systems[6]. Here we show that such an interesting joining behavior of singular lines can also occur for NILs, for example

$$f_2(\mathbf{k}) = k_x k_z, \quad f_3(\mathbf{k}) = -k_x^2 + k_y^2 + k_z^2 - d, \tag{5}$$

The Hamiltonian exihibits a chain-like structure in **k**-space, which is composed of a circular NIL located on the k_x=0 plane that is chained to two hyperbolic NILs locating on the k_z=0 plane at two intersecting points, as depicted in Fig. 3a1. All the NILs (satisfy the certain condition $f_2 = f_3 = 0$) are adjacent to

ESs, which are represented by the red (ES_1) and green (ES_2) surfaces (satisfy $f_2 = \mp f_3$, respectivley), corresponding to EL_1 and EL_2 in Fig. 1, respectively. We begin by examining the loop l_6, which encloses the waists of two ESs and their NILs, but does not cut through any ESs. According to our previous analysis, such a loop is trivial. This may not be immediately apparent from the figure, as the ESs and NILs seem to prevent the loop from retracting to a point. However, by changing d from positive to negative, the waists of ESs and NIL gradually retract to a point (as shown in Fig. 3b1), and finally open up to form a gap (as shown in Fig. 3c1). The two NILs enclosed by the loop can thus annihilate each other, providing solid evidence that l_6 is indeed a trivial loop. The trivial loop l_6 enforces the ESs connecting the two NILs to remain smooth as the Hamiltonian deforms. This can be explained by l_6' (see Fig. 3a1), which is homotopic to l_6, as they enclose the same NILs, but l_6' traverses ESs. On the cross section plane that l_6' lies on, l_6' is segmented by ESs into several paths, where the red and green lines denote ES_1 and ES_2 cut by the plane, as sketched in Fig. 3a2. The topological invariants on the segments of l_6' must cancel each other to form a trivial product, implying that the path l_t, which are terminated at ESs, must carry a trivial topological invariant. This can be directly seen from Figs. 3a1-a2, where the path l_t has two terminal points attached to the same smooth ES without cutting through the other kind of ES (similar to l_1, l_2 and l_4 in Fig. 2). As one continues to deform the Hamiltonian (d<0), the two ESs enclosed become disconnected after the two NILs annihilate (see Fig. 3c1-c2). Moving on to the loop l_2 in Fig. 3a1, we see that it is segmented by the ESs into different paths, as depicted in Fig. 3a3. The loop can be represented as a combination of paths $(\beta^{-1}\alpha^{-1}\beta'^{-1}\alpha'^{-1})^2$, carrying a nontrivial squared topological invariant $(Z_1^{-1}Z_3^{-1})^2$. This invariant prevents the two encircled NILs to annihilate each other as d varies in the Hamiltonian [Eq. (5)]. The two NILs merge at a point for d=0 (Fig. 3b1), dividing the nearby area into eight regions (see Fig. 3b3). Since the loop is still the combination $(\beta^{-1}\alpha^{-1}\beta'^{-1}\alpha'^{-1})^2$, the topological invariant remains to be squared $(Z_1^{-1}Z_3^{-1})^2$ and does not change. As d varies, the point splits, and the two NILs become separate in opposite directions, as shown in Figs. 3c1, c3. Thus, the squared invariant $(Z_1^{-1}Z_3^{-1})^2$ is conserved within the deformation of the Hamiltonian. *The conservation of the squared invariant $(Z_1^{-1}Z_3^{-1})^2$ on l_7 and the trivial invariant on l_6 (or l_6') is a necessary condition for the*

chain of NILs. Periodic systems with nonreciprocal hoppings can implement the chain of NILs in band structures, as described in Section 5 of the supplementary information. We note that the chain-like structure of NILs is not stable against perturbations to the Hamiltonian (as indicated by Fig. 3). In addition, breaking the mirror symmetries $k_x \rightarrow -k_x$ and $k_z \rightarrow -k_z$ also eliminate the chain-like structure. We illustrate this in Section 5 of supplementary information. The invariant conservation shows that two inannihilable NILs cannot be directly connected by smooth ESs, as can be observed in Fig. 3a3-c3.

We next demonstrate that the NIL (or NIP) can host topologically protected edge states, representing a novel type of bulk-edge correspondence in a gapless non-Hermitian system. This concept may seem counterintuitive, as bulk-edge correspondence is typically discussed in gapped phases[8,11]. Specifically, we consider the following 1D **k**-space Hamiltonian corresponding to a lattice model,

$$H(k) = \sigma_3 \cos k + i\sigma_2 \sin k + v\sigma_0 \cos(k + a) \tag{6}$$

where σ_0 is the 2 by 2 identity matrix. The Hamiltonian includes term proportional to σ_0, which is useful in tuning bandgaps to identify edge states. Introducing the identity term does not change the topology of the system, and the degeneracy features remain unchanged. By making a comparison to Eq. (1), we have the following correspondence: $f_3(k)=\cos k$ and $f_2(k)=\sin k$. The path traced out by $(f_2(k), f_3(k))$ goes around the NIP as shown in Fig. 4a, and we can see that the 1D Brillouin zone of the lattice model carries the topological invariant Z_1Z_3. Such a Hamiltonian can be realized by the 1D periodic system in Fig. 4b, and the corresponding real space Hamiltonian is

$$H_r = \underbrace{\frac{1}{2}(\sigma_3 + \sigma_2 + ve^{ia}\sigma_0)}_{t_1} \sum\nolimits_j c_j^\dagger c_{j+1} + \underbrace{\frac{1}{2}(\sigma_3 - \sigma_2 + ve^{-ia}\sigma_0)}_{t_2} \sum\nolimits_j c_j^\dagger c_{j-1} \tag{7}$$

where j denotes unit cell index. The hopping of obitals is described by two 2×2 hopping matrices, t_1 and t_2, whose elements represent the hopping parameters between lattice sites, as shown in Fig. 4b. The hopping matrices satisfy the relation $t_1^* = t_2$. As the 1D Brillouin zone inevitably cut through the ELs four times, the band structure undergoes line gap closing four times, as shown in Fig. 4c. Obviously, the conventional Zak phase, which is commonly used for explaining edge states in gapped 1D systems, cannot be defined in this 1D Brillouin zone. However, the two eigenstates experience frame deformation

process along each paths, and evolve from parallel states to anti-parallel states (Fig. S3b2 in supplementary information) along each path. This process shows that the relative rotation angle between the two eigenstates is π, which is equal to an integral

$$\psi = \oint_{l_\alpha} i\langle\varphi|\nabla_k\varphi\rangle dk \tag{8}$$

The loop l_α in the integration (Eq. 8) is shown in Fig. 4d, and connects the trajectories of the two eigenvalues on path α at ELs. In this context, this loop l_α is in the 3D Re(E)-f_2-f_3 space. Moreover, Eq. (8) represents the conventional Berry phase, which is related to the frame deformation on path α. On path α', the two eigenstates swap compared with path α, resulting in a relative rotation angle of $-\pi$, which means that the Berry phase along the loop $l_{\alpha'}$ is $-\pi$ (see Fig. 4d). Additionally, the identity term in the Hamiltonian [Eq. (6)] creates a real line gap between the eigenenergies on path α and path α'. As a result, if we truncate the 1D system with open boundaries, there will be a pair of edge modes residing in the line gap, as shown in Fig. 4e, where the black and red dots represent the projection bands under open boundary condition (OBC) and periodic boundary condition (PBC). In broken phases, the eigenenergies form point gaps in the projection band, which lead to the skin effect as indicated in Fig. 4e. The edge states are separate from any bulk modes and skin modes, making them easily distinguishable. The field distribution (amplitude $|\varphi|$) of one edge mode is shown in Fig. 4f, and it is obvious that the field is confined at the left edge of the 1D chain (inset).

To summarize, we have topologically classified a generic non-Hermitian two-level system possessing *PT* symmetry and an additional pseudo-Hermitian symmetry that may arise in systems with non-reciprocal hoppings[41,46-48]. These systems feature surfaces of exceptional points that host stable embedded intersection singularities in momentum space. Our study demonstrates that the topology of this gapless structure can be understood by examining the quotient space under equivalence relations of eigenstates, which is a bouquet of three circles. The fundamental group of this space is isomorphic to a free non-Abelian group on three generators, which allow us to predict the formation and evolution of chain-like structures of NILs as the Hamiltonian deforms, based on the conservation of topological

invariants. Our work further predicts the existence of topologically protected edge states, which is a remarkable and counter-intuitive phenomenon for such gapless phases. The method of quotient space topology might potentially be extended to classify other hypersurface singularities in non-Hermitian systems, such as high-order exceptional points as cusps[32,40] and more complicated swallowtail catastrophes[41]. Our work also propose a new kind of non-Hermitian gapless topological phase of matter, providing pathways for designing systems to realize robust topological non-defective degeneracies in non-Hermitian systems.

Acknowledgements: This work is supported by Research Grants Council of Hong Kong through grants AoE/P-502/20, 16307621, 16307821, 16307420, 16310420 and Croucher Foundation (CAS20SC01) and KAUST20SC01. Y. Zhu acknowledges the financial support from National Natural Science Foundation of China (NSFC) grant 11701263.

Author contributions: H.J. and C.T.C. planned the project. H.J., R.Y.Z., Y.Z. constructed the theoretical framework. H.J., R.Y.Z., Y.Z., and C.T.C. wrote the manuscript. All authors contributed to the discussion.

Competing interests: The authors declare no competing interests.

Data and codes are available in this work.

Additional Information:

Supplementary Information is available for this paper.

Correspondence and requests for materials should be addressed to: zhuyf@sustech.edu.cn; phchan@ust.hk.

References:

1. Lu, L., Fu, L., Joannopoulos, J. D., et al., Weyl points and line nodes in gyroid photonic crystals, *Nat. Photon.* **7**, 294-299 (2013).

2. Lu, L., Joannopoulos, J. D., Soljačić, M., Topological photonics, *Nat. Photon.* **8**, 821-829 (2014).

3. Abanin, D. A., Morozov, S. V., Ponomarenko, L. A., et al. Giant nonlocality near the Dirac point in graphene, *Science* **332**, 328-330 (2011).

4. Jiang, Z., Zhang, Y., Stormer, H. L., et al. Quantum Hall states near the charge-neutral Dirac point in graphene, *Phys. Rev. Lett.* **99**, 106802 (2007).

5. Lu, L., Wang, Z., Ye, D., et al. Experimental observation of Weyl points, *Science* **349**, 622-624 (2015).

6. Wu, Q. S., Soluyanov, A. A., Bzdušek, T., Non-Abelian band topology in noninteracting metals, *Science* **365**, 1273-1277 (2019).

7. Yang, E., Yang, B., You, O., et al. Observation of non-Abelian nodal links in photonics, *Phys. Rev. Lett.* **125**, 033901 (2020).

8. Guo, Q., Jiang, T., Zhang, R. Y., et al. Experimental observation of non-Abelian topological charges and edge states, *Nature* **594**, 195-200 (2021).

9. Soluyanov, A. A., Gresch, D., Wang, Z., et al. Type-ii weyl semimetals, *Nature* **527**, 495-498 (2015).

10. Yang, L. X., Liu, Z. K., Sun, Y., et al. Weyl semimetal phase in the non-centrosymmetric compound TaAs, *Nat. Phys.* **11**, 728-732 (2015).

11. Yang, B., Guo, Q., Tremain, B., et al. Ideal Weyl points and helicoid surface states in artificial photonic crystal structures, *Science* **359**, 1013-1016 (2018).

12. Jia, H., Zhang, R., Gao, W., et al. Observation of chiral zero mode in inhomogeneous three-dimensional Weyl metamaterials, *Science* **363**, 148-151 (2019).

13. Jia, H., Zhang, R. Y., Gao, W., et al. Chiral transport of pseudospinors induced by synthetic gravitational field in photonic Weyl metamaterials, *Phys. Rev. B* **104**, 045132 (2021).

14. Gong, Z., Ashida, Y., Kawabata, K., et al. Topological phases of non-Hermitian systems, *Phys. Rev. X* **8**, 031079 (2018).

15. Yao, S., Wang, Z., Edge states and topological invariants of non-Hermitian systems, *Phys. Rev. Lett.* **121**, 086803 (2018).

16. Shen, H., Zhen, B., Fu, L., Topological band theory for non-Hermitian Hamiltonians, *Phys. Rev. Lett.* **120**, 146402 (2018).

17. Okuma, N., Kawabata, K., Shiozaki K., et al. Topological origin of non-Hermitian skin effects, *Phys. Rev. Lett.* **124**, 086801 (2020).

18. Leykam, D., Bliokh, K. Y., Huang, C., et al. Edge modes, degeneracies, and topological numbers in non-Hermitian systems, *Phys. Rev. Lett.* **118**, 040401 (2017).

19. Bergholtz, E. J., Budich, J. C., Kunst, F. K., Exceptional topology of non-Hermitian systems, *Rev. Mod. Phys.* **93**, 015005 (2021).

20. Kawabata, K., Shiozaki, K., Ueda, M., et al. Symmetry and topology in non-Hermitian physics, *Phys. Rev. X* **9**, 041015 (2019).

21. Borgnia, D. S., Kruchkov, A. J., Slager, R. J., Non-Hermitian boundary modes and topology, *Phys. Rev. Lett.* **124**, 056802 (2020).

22. Kawabata, K., Bessho, T., Sato, M., Classification of exceptional points and non-Hermitian topological semimetals, *Phys. Rev. Lett.* **123**, 066405 (2019).

23. Song, F., Yao, S., Wang, Z., Non-Hermitian topological invariants in real space, *Phys. Rev. Lett.* **123**, 246801 (2019).

24. Zhou, H., Peng, C., Yoon, Y., et al. Observation of bulk Fermi arc and polarization half charge from paired exceptional points, *Science* **359**, 1009-1012 (2018).

25. Helbig, T., Hofmann, T., Imhof, S., et al. Generalized bulk–boundary correspondence in non-Hermitian topolectrical circuits, *Nat. Phys.* **16**, 747-750 (2020).

26. Wang, K., Dutt, A., Wojcik, C. C., et al. Topological complex-energy braiding of non-Hermitian bands, *Nature* **598**, 59-64 (2021).

27. Zhou, H, Lee, J. Y., Liu, S., et al. Exceptional surfaces in PT-symmetric non-Hermitian photonic systems, *Optica* **6**, 190-193 (2019).

28. Okugawa, R., Yokoyama, T., Topological exceptional surfaces in non-Hermitian systems with parity-time and parity-particle-hole symmetries, *Phys. Rev. B* **99**, 041202 (2019).

29. Zhang, X., Ding, K., Zhou, X., et al. Experimental observation of an exceptional surface in synthetic dimensions with magnon polaritons. *Phys. Rev. Lett.* **123**, 237202 (2019).

30. Yang, Z., Hu, J., Non-Hermitian Hopf-link exceptional line semimetals, *Phys. Rev. B* **99**, 081102 (2019).

31. Zhong, Q., Ren, J., Khajavikhan, M., et al. Sensing with exceptional surfaces in order to combine sensitivity with robustness, *Phys. Rev. Lett.* **122**, 153902 (2019).

32. Tang, W., Jiang, X., Ding, K., et al. Exceptional nexus with a hybrid topological invariant. *Science* **370**, 1077-1080 (2020).

33. Wojcik, C. C., Sun, X. Q., Bzdušek, T., et al. Homotopy characterization of non-Hermitian Hamiltonians, *Phys. Rev. B* **101**, 205417 (2020).

34. Sun, X. Q., Wojcik, C. C., Fan, S., et al. Alice strings in non-Hermitian systems, *Phys. Rev. Res.* **2**, 023226 (2020).

35. Li, Z., Mong, R. S. K., Homotopical characterization of non-Hermitian band structures, *Phys. Rev. B* **103**, 155129 (2021).

36. Soleymani, S., Zhong, Q., Mokim, M., et al. Chiral and degenerate perfect absorption on exceptional surfaces. Nat. Commun. **13**, 599 (2022).

37. Xiao, Y. X., Ding, K., Zhang, R. Y., et al. Exceptional points make an astroid in non-Hermitian Lieb lattice: Evolution and topological protection, *Phys. Rev. B* **102**, 245144 (2020).

38. Sayyad, S., Stalhammar, M., Rodland, L., et al. Symmetry-protected exceptional and nodal points in non-Hermitian systems, arXiv preprint arXiv:2204.13945, 2022.

39. Zhang, R. Y., Cui, X., Chen, W. J., et al. Symmetry-protected topological exceptional chains in non-Hermitian crystals, arXiv preprint arXiv:2204.08052, 2022.

40. Delplace, P., Yoshida, T., Hatsugai, Y., Symmetry-protected multifold exceptional points and their topological characterization, *Phys. Rev. Lett.* **127**, 186602 (2021).

41. Hu, J., Zhang, R. Y. et al. Non-Hermitian swallowtail catastrophe revealing transitions across diverse topological singularities, Research Square preprint [https://doi.org/10.21203/rs.3.rs-1853770/v1] (2022).

42. Mostafazadeh, A., Pseudo-Hermitian representation of quantum mechanics, *Int. J. Geo. Meth. Mod. Phys.* **7**, 1191-1306 (2010).

43. Mostafazadeh, A., Quantum brachistochrone problem and the geometry of the state space in pseudo-Hermitian quantum mechanics, *Phys. Rev. Lett.* **99**, 130502 (2007).

44. Freedman, D. Z., Van Proeyen, A., Supergravity, Cambridge university press, 2012.

45. Frankel, T., The geometry of physics: an introduction, Cambridge university press, 2011.

46. Buddhiraju, S., Song, A., Papadakis, G. T., et al. Nonreciprocal metamaterial obeying time-reversal symmetry, *Phys. Rev. Lett.* **124**, 257403 (2020).

47. Wang, X., Ptitcyn, G., Asadchy, V. S., et al. Nonreciprocity in bianisotropic systems with uniform time modulation, *Phys. Rev. Lett.* **125**, 266102 (2020).

48. Ezawa, M., Non-Hermitian non-Abelian topological insulators with PT symmetry, *Phys. Rev. Res.* **3**, 043006 (2021).

49. Spanier, E. H., Algebraic topology, Springer Science & Business Media, 1989.

50. Gajer, P., The intersection Dold-Thom theorem, *Topology* **35**, 939-967 (1996).

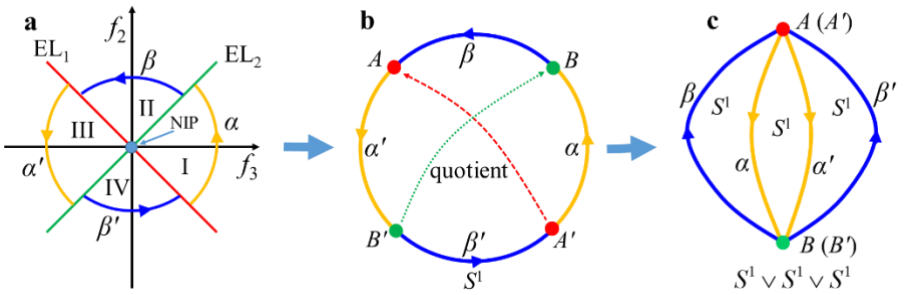

Fig. 1| Construction of quotient space under equivalence relations. a The gapless structure of parameter space, where EL_1 and EL_2 characterize exceptional lines satisfying $f_2 = \mp f_3$, respectively. The NIP is at the origin where the ELs intersect f_2=f_3=0.. Regions I and III are *PT*-exact phases, and Regions II and IV are *PT*-broken phases. **b** The 2D plane excluding the NIP can deformation retract to a circle S^1, with the upper and lower parts of EL_1 shrinking to A and A', respectively. Similarly upper and lower parts of EL_2 shrink to B and B', respectively. **c** Gluing identified points A with A', and B with B', the quotient space of S^1 in panel **b** can be obtained as a bouquet of three circles.

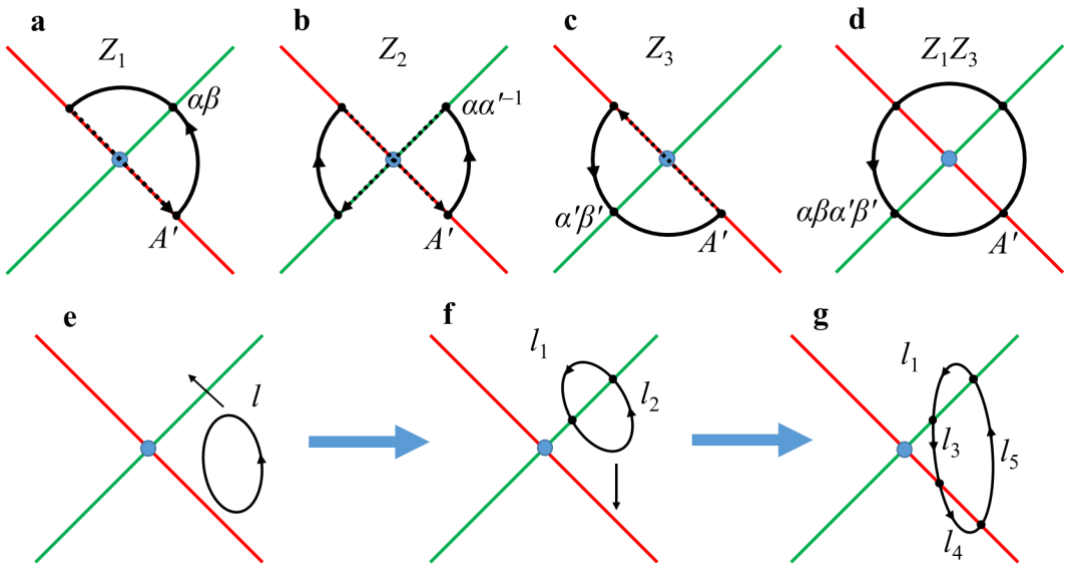

Fig. 2| Typical loops carrying non-trivial or trivial topological invariants. a-c Loops carrying nontrivial topological invariants Z_1, Z_2 and Z_3 respectively, being generators in the group (Eq. 4). The dashed lines with arrows denote quotient maps, i.e. gluing identified points. **d** The loop formed by the combination $\alpha\beta\alpha'\beta'$ encloses the NIP, which carries the topological invariant Z_1Z_3. Point A' in panels **a-d** denotes the basepoint. **e-g** Evolution of a loop carrying trivial topological charge. **e** A loop without touching ELs is confined within a specific region and is trivial. **f** Moving the loop l in panel **e** along the black arrow direction, the loop becomes a composite of paths l_1 and l_2. Both of l_1 and l_2 are trivial loops in the quotient space M, and thus the loop due to their composition is also trivial. **g** Stretching the loop along the black arrow direction in panel **f**, the loop crosses EL_1 and becomes a composite of paths $l_1l_3l_4l_5$. The path l_4, similar to l_1 and l_2, corresponds to a trivial loop in quotient space M. The paths l_5 and l_3 are oriented in opposite directions (labelled by the arrows), and are homotopic to α and α^{-1}, respectively. The path product $l_1l_3l_4l_5$ is thus trivial.

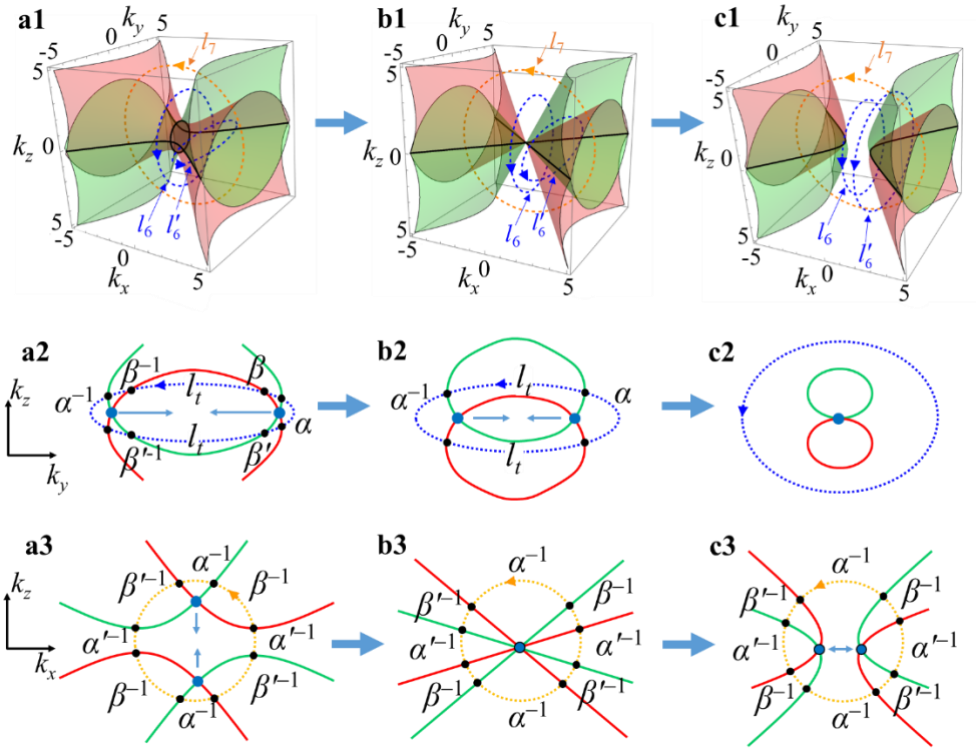

Fig. 3| Explaining the formation of the chain of NILs in k-space and its evolution against perturbations with the fundamental group. a1-c1 ESs (red and green surfaces) and NILs (black lines) plotted with Eq. 5, corresponding to $d > 0$, $d = 0$ and $d < 0$, respectively. The blue loops l_6 and l_6' have trivial topological invariants. **a2-c2** Cross section of the plane that l_6' locates on. The enclosed pair of NILs can annihilate each other. The path l_t is a path with its terminal points on the same ES without cutting through the other kind of ES. Similar to l_1, l_2 and l_4 in Fig. 2, l_t also carries a trivial topological invariant, and thus the subscript t means trivial. **a3-c3** Cross section of the plane that the orange l_7 locates on. The NILs enclosed cannot annihilate each other. Red and green lines: ESs; Dark blue dots: NILs; Black dots: intersecting points of loops on ESs (in Row 2 and Row 3).

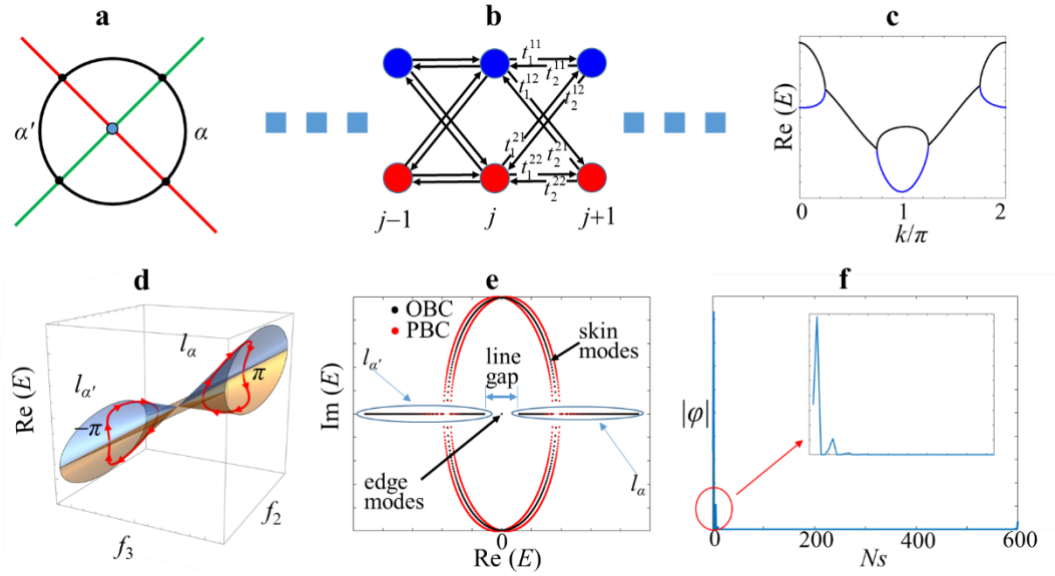

Fig. 4| Topologically protected edge states by invariant Z_1Z_3. a A loop circulating the NIP, being the Brillouin zone of the 1D lattice model in Eq. 6, is partitioned into four paths, with α and α' residing in exact phases. **b** Realization of the lattice model. The hopping parameters $t_{1,2}^{11}$, $t_{1,2}^{12}$, $t_{1,2}^{21}$ and $t_{1,2}^{22}$ are the entries of the hopping metrices t_1 or t_2 in Eq. (7). **c** Eigenvalue dispersions (real part) of the model Eq. (7) in the 1D Brillouin zone. Since the Brillouin zone cuts through ELs four times, the band structure experience gap closing four times. **d** Joining the trajectories of two bands on path α forms a loop in Re(ω)-f_2-f_3 space l_α, along which the Berry phase is π. This quantized Berry phase is equal to the relative rotation angle of the two eigenstates due to frame deformation on path α. For path α', joining the two bands forms the loop $l_{\alpha'}$, along which the Berry phase is $-\pi$. This is because the two eigenstates swap on path α' (compared with path α) due to band inversion at NIP, the relative rotation angle of the eigenstates changes the sign. **e** Plots of projection bands of the 1D lattice model under open boundary conditions (OBC, black dots) and periodic boundary conditions (PBC, red dots). There exist a pair of edge modes in the line gap for eigenstates on loops l_α and $l_{\alpha'}$ in panel **d**. **f** Field distribution of one edge mode. The lattice model with OBC has 300 periods (600 lattice sites, denoted by *Ns*). Inset: zoom-in view showing the field distribution near the left edge.

Supplementary material: Topological classification for intersection singularities of exceptional surfaces in pseudo-Hermitian systems

Hongwei Jia[#], Ruo-Yang Zhang[#], Jing Hu, Yixin Xiao, Shuang Zhang, Yifei Zhu[*], C. T. Chan[†]

1. Pseudo-Hermiticity and metric operator

The pseudo-Hermiticity can be regarded as a symmetry in non-Hermitian physics [1], and a formal definition of pseudo-Hermiticity is always accompanied with a metric operator η

$$\eta H \eta^{-1} = H^{\dagger} \tag{S1}$$

Hence, a pseudo-Hermitian system is also called a η-pseudo-Hermitian system, and the metric operator η is a Hermitian matrix. Recently, the parity-time inversion symmetry (*PT*) is included in pseudo-Hermiticity symmetry [2,3]. The considered system thus includes two inequivalent pseudo-Hermitian symmetries. In quantum mechanics, the Hamiltonians of two systems can be considered to be equivalent if they can transform to each other via unitary transformations ($U^{-1} = U^{\dagger}$)

$$H\varphi = E\varphi \rightarrow UHU^{\dagger}U\varphi = EU\varphi \rightarrow H'\varphi' = E\varphi' \tag{S2}$$

We apply the transformation to Eq. S1

$$\begin{aligned} & U\eta H\eta^{-1}U^{\dagger} = UH^{\dagger}U^{\dagger} \\ & \rightarrow U\eta U^{\dagger}UHU^{\dagger}U\eta^{-1}U^{\dagger} = UH^{\dagger}U^{\dagger} \\ & \rightarrow \eta' H' \eta'^{-1} = H'^{\dagger} \end{aligned} \tag{S3}$$

where $\eta' = U\eta U^{\dagger}$ is the transformed metric operator. For the considered system in Eq. (S2), one can apply an SU(2) transformation to the Hamiltonian, e.g.

$$\begin{aligned} & H' = e^{i\frac{\theta}{2}\sigma_1} H e^{-i\frac{\theta}{2}\sigma_1} \\ & = (f_2(\mathbf{k})i\sigma_2 + f_3(\mathbf{k})\sigma_3)\cos\theta + (-f_2(\mathbf{k})i\sigma_3 + f_3(\mathbf{k})\sigma_2)\sin\theta \end{aligned} \tag{S4}$$

It is found that the Hamiltonian can be transformed to a *PT*-symmetric system with equal gain and loss for $\theta = \pi/2$,

$$H' = -f_2(\mathbf{k})i\sigma_3 + f_3(\mathbf{k})\sigma_2 \tag{S5}$$

and the metric operator is simultaneously transformed to

$$\eta' = \begin{bmatrix} 0 & i \\ -i & 0 \end{bmatrix} \tag{S6}$$

Hence, the classification in this work can be extended to other *PT*-symmetric pseudo-Hermitian systems (e.g. realized by equal gain and loss, Eq. S5) with equivalent metric operators [4].

2. Quotient space and stratified space

In topology, the quotient space of a topological space under given equivalence relations is a new topological space constructed by endowing the quotient set of the original topological space with the

quotient topology [5]. Let (X, τ_X) be a topological space, and let ~ be equivalent relation on X. The quotient set $Y=X/\sim$ is the set of equivalence classes of elements of X. The equivalence class of $x \in X$ is denoted by $[x]$. The quotient map associated with ~ refers to the surjective map

$$\begin{aligned} q: X &\to X/\sim \\ x &\to [x] \end{aligned} \tag{S7}$$

Intuitively speaking, all points in each equivalence class are identified or glued together. A well-known example of quotient space is the Brillouin zone. In the momentum space of periodic systems, a point $\mathbf{k}$ is identified with points $\mathbf{k}+m_a\mathbf{G}_a$ because a $\mathbf{k}$-space Hamiltonian at these points have the same eigenvalues and eigenstates. Here $\mathbf{G}_a$ are reciprocal lattice vectors and m_a are integers. That is why we mostly considers the band dispersions in the first Brillouin zone. It is also notable that the points on one side of the Brillouin zone boundaries can be translated to the points on the other boundary under translational operations of $\mathbf{G}_a$. Such points are identified and can be glued together. As simple examples, the first Brillouin zone is a quotient map of the momentum space under equivalence relation of translations by $\mathbf{G}_a$, and points in the first Brillouin zone are the representatives of all the equivalence classes. For 1D periodic systems, identifying points on the first Brillouin zone boundary constructs a quotient space, which is a 1D circle S^1 (see Fig. S1a1-a2). Similarly, opposite edges (p_1 and p_2, and p_3 and p_4) of the Brillouin zone of 2D periodic systems can be identified (see Fig. S1b1). By gluing p_1 to p_2, the Brillouin zone becomes a cylinder (see Fig. S1b2). We further glue p_3 to p_4, and the cylinder becomes a torus T (see Fig. S1b3). p_1 (or p_2) and p_3 (or p_4) are called the skeleton of the torus, and is a bouquet of two circles with a common basepoint $S^1 \vee S^1$. The surface of the torus is called the two-cell. Assembling the skeleton and the two-cell, the torus can be described by the product $T = S^1 \times S^1$. The topology of the torus is thus described by its fundamental group $\pi_1(T) = \mathbf{Z} \times \mathbf{Z}$. This is a free Abelian group on two generators.

The momentum space of the considered system is a stratified space [6,7]. In topology, a stratified space is a triple (V,S,ζ), where V is a topological space (often we require it to be locally compact, Hausdorff, and second countable), S is a decomposition of V into strata $V = \bigcup_{X \in S} X$, and ζ is the set of control data $\{(T_X),(\pi_X),(\rho_X)|X \in S\}$, where T_X is an open neighborhood of the stratum X, π_X: $T_X \to X$ is a continuous retraction, and ρ_X: $T_X \to [0,+\infty)$ is a continuous function. These data need to satisfy the following conditions:

1. Each stratum X is a locally closed subset and the decomposition S is locally finite.

2. The decomposition S satisfies the axiom of the frontier: if X, $Y \in S$ and $Y \cap \bar{X} \neq \varnothing$, then $Y \subset \bar{X}$. The condition implies that there is a partial order among strata: $Y<X$ if and only if $Y \subset \bar{X}$ and $Y \neq X$.

3. Each T_X is a smooth manifold.

4. $X=\{v \in T_X | \rho_X(v)=0\}$. So ρ_X can be viewed as the distance function from the stratum X.

5. For each pair of strata $Y<X$, the restriction (π_X, ρ_X): $T_Y \bigcap X \to Y \times (0,+\infty)$ is a submersion.

6. For each pair of strata $Y<X$, there holds $\pi_Y \circ \pi_X = \pi_Y$ and $\rho_Y \circ \pi_X = \rho_Y$.

Consider the parameter space f_2-f_3 of our Hamiltonian, the topological space V is simply the plane (Fig. S2). Thus S is the decomposition of V into three strata (X, Y, Z), which are the 2D space R^2 (X), the singular hypersurfaces ELs at $f_2 = \pm f_3$ (Y=Sing(X)), and the hypersurface singularity NIP (Z=Sing(Sing(X))) at the center, as shown in Fig. S2. For each stratum (e.g. X), the smooth manifold T_X

considers the nearby neighborhood. Therefore, T_1-T_3 in Fig. S2 correspond to the three strata *X*, *Y* and *Z*, respectively.

Our classification is based on eigenstates. The Hamiltonian in spaces without gap closing can be expressed with the sum

$$H = \sum_{i=1,2} E_i \left|\varphi_i^L\right\rangle\left\langle\varphi_i^R\right| \tag{S8}$$

where $\varphi_i^{L(R)}$ denote the left and right eigenstates of the Hamiltonian. The pseudo-Hermiticity and *PT* symmetries of the system enforces the left and right eigenstates (both in exact and broken phases) to be connected by the following relation

$$\varphi_i^L = \eta(\varphi_i^R)^* \tag{S9}$$

The quotient space is constructed by identifying points with the same eigenstates. Note that the eigenstates are ordered by the corresponding eigenvalues, and the criterion for ordering eigenstates has been introduced in the maintext. Hence, gluing point *A′* and point *A*, and *B* to *B′* is understandable, because the two eigenstates at these points coalesce, and ordering eigenstates is meaningless at these points.

$$\begin{aligned} \varphi_1 = \varphi_2 = \begin{bmatrix} -1 \\ 1 \end{bmatrix} \qquad & for \quad f_2 = f_3 \\ \varphi_1 = \varphi_2 = \begin{bmatrix} 1 \\ 1 \end{bmatrix} \qquad & for \quad f_2 = -f_3 \end{aligned} \tag{S10}$$

However, in spaces without gap closing, by adding a minus sign to the Hamiltonian in Eq. S8, both eigenenergies take negative signs, and the eigenstates remain the same. This process can be realized by taking the negatives of f_2 and f_3, which are just the antipodal points lying in opposite regions with respect to the NIP. Even though the two points have the same eigenstates, the order of the two states exchanges for antipodal points because eigenvalues are added by minus signs. Therefore, the two points cannot be identified, which is distinct from the points on ELs. The constructed space Eq. (3) in the main text is a stratified quotient space, and the corresponding topology Eq. (4) is thus a quotient space topology. Since the nontrivial loops in parameter (or quotient) space all traverses the singular hypersurfaces (i.e. EL or ES), our approach is affiliated to the intersection homotopy theory [6].

3. Frame deformation of eigenstates

The metric operator for pseudo-Hermiticity plays a similar role as the space-time metric in general relativity [8,9], and the eigenstates are like local coordinate frames (or tetrad). The local metric *g* can be defined with the indefinite inner product $g_{mn} = \langle\varphi_m \,|\, \eta\varphi_n\rangle$ [10]. In our previous work discussing the topology of swallowtail catastrophes in non-Hermitian systems [10], we established the relationship between the local metric *g* and the geometric phase. Here we repeat the derivation details. The evolution problem is governed by the equation

$$H\left|\varphi_m\right\rangle = i\partial_\zeta \left|\varphi_m\right\rangle \tag{S11}$$

where ζ denotes a path parameter, and φ_m are the eigenstates. The completeness of eigenstates (off ES) shows that any field can be expanded as

$$\phi_n(\lambda(\zeta)) = \sum_m [U(\lambda(\zeta))]^{-1}{}_n{}^m \varphi_m(\lambda(\zeta)) \tag{S12}$$

where λ denotes the parameter space of the Hamiltonian with components $\lambda^1, \lambda^2, \lambda^3 \ldots$. It is not difficult to find that ϕ_n is also the solution of Eq. S11. In static evolution problems, $\phi_n(\lambda(\zeta))$ represents $\varphi_n(\lambda(\zeta + \delta\zeta))$. Applying the partial derivative with respect to ζ, one obtains

$$\begin{aligned} i\frac{\partial}{\partial\zeta}\phi_n(\lambda(\zeta)) &= H[U(\lambda(\zeta))]^{-1}{}_n{}^m \varphi_m(\lambda(\zeta)) \\ &= i\frac{\partial[U(\lambda(\zeta))]^{-1}{}_n{}^m}{\partial\zeta}\varphi_m(\lambda(\zeta)) + i[U(\lambda(\zeta))]^{-1}{}_n{}^m \frac{\partial\varphi_m(\lambda(\zeta))}{\partial\zeta} \end{aligned} \tag{S13}$$

The instantaneous eigenvalue problem

$$H(\lambda(\zeta))\varphi_m(\lambda(\zeta)) = E_m\varphi_m(\lambda(\zeta)) \tag{S14}$$

and applying a scalar product by the left eigenstate $\langle\varphi_l'|$ from the left of Eq. S13 yields

$$-iE_l[U(\lambda(\zeta))]^{-1}{}_n{}^l = \frac{\partial[U(\lambda(\zeta))]^{-1}{}_n{}^l}{\partial\zeta} + \langle\varphi_l'|\frac{\partial|\varphi_m(\lambda(\zeta))\rangle}{\partial\zeta}[U(\lambda(\zeta))]^{-1}{}_n{}^m \tag{S15}$$

The partial derivative with respect to ζ can be expanded as

$$\frac{\partial|\varphi_m(\lambda(\zeta))\rangle}{\partial\zeta} = \sum_k \frac{\partial|\varphi_m(\lambda(\zeta))\rangle}{\partial\lambda^k}\frac{\partial\lambda^k}{\partial\zeta}, \quad (k = 1, 2, 3\ldots) \tag{S16}$$

We define the affine connection

$$A_k{}^n{}_m = -\langle\varphi_n'|\frac{\partial|\varphi_m(\lambda(\zeta))\rangle}{\partial\lambda^k} = -\langle\varphi_n'|\frac{\partial}{\partial\lambda^k}|\varphi_m\rangle \tag{S17}$$

and the solution to U^{-1} is thus obtained as

$$U^{-1} = \mathrm{P}\exp[\int_0^\zeta ds\frac{\partial\lambda^k}{\partial s}A_k - i\int_0^\zeta dsE(\lambda(s))] = \mathrm{P}\exp(\int_{\lambda(0)}^{\lambda(\zeta)} d\lambda^k A_k)\times\exp[-i\int_0^\zeta dsE(\lambda(s))] \tag{S18}$$

Ignoring the dynamical phase, the geometric phase is simply

$$U^{-1} = \mathrm{P}\exp(\int_{\lambda(0)}^{\lambda(\zeta)} d\lambda^k A_k) \tag{S19}$$

where P denotes path ordering operator, which is important here, because the affine connection *A* is a matrix. Considering the non-commutative nature of matrix product, *A* is a non-Abelian parallel transport gauge, and the integration of *A* on closed loops depends on the path circulating singularities. Here we define a local metric *g* with its elements being

$$g_{mn} = \langle\varphi_m|\eta\varphi_n\rangle \tag{S20}$$

which has explicit relations with the affine connection. The symmetries (Eq. 1 in the maintext) of the Hamiltonian provide an important relation between the left and right eigenstates

$$\varphi'_m = \varphi_m^T \eta \text{ (or equivalently, } \varphi_m'^T = \eta\varphi_m,\ \langle\varphi'_m| = \langle\varphi_m^*|\eta\ ,\ |\varphi'_m\rangle = \eta|\varphi_m^*\rangle \tag{S21}$$

This relation provides an orthogonality to the right eigenstates

$$\varphi_m^T \eta \varphi_n \begin{cases} = 0 & m \neq n \\ \neq 0 & m = n \end{cases} \tag{S22}$$

The orthogonal relation shows that the arbitrary phase can always be removed by normalizing the eigenstates (up to an unfixed sign)

$$\varphi_m \to \frac{\varphi_m}{\sqrt{\varphi_m^T \eta \varphi_m}} \tag{S23}$$

The normalization of eigenstates can make g a constant matrix and thus the partial derivative with respect to the path parameter vanishes

$$0 = \partial_\zeta g_{mn} = \partial_\zeta \langle\varphi_m | \eta\varphi_n\rangle \tag{S24}$$

Inserting the identity operator $I = \sum_l |\varphi'_l\rangle\langle\varphi_l| = \sum_l |\varphi_l\rangle\langle\varphi'_l|$, one obtains

$$\partial_{\lambda_k} \langle\varphi_m | \eta\varphi_n\rangle = \sum_l \langle\partial_{\lambda_k}\varphi_m|\varphi'_l\rangle\langle\varphi_l|\eta\varphi_n\rangle + \sum_l \langle\varphi_m|\eta|\varphi_l\rangle\langle\varphi'_l|\partial_{\lambda_k}\varphi_n\rangle \tag{S25}$$

We note that

$$\langle\partial_{\lambda_k}\varphi_m|\varphi'_l\rangle = \langle\partial_{\lambda_k}\varphi_m|\eta\varphi_l^*\rangle = \langle\varphi_l^*|\eta|\partial_{\lambda_k}\varphi_m\rangle^* = \langle\varphi'_l|\partial_{\lambda_k}\varphi_m\rangle^* \tag{S26}$$

And thus relationship between the metric g and the affine connection of the geometric phase

$$A^{*l}_{k_i\ m} g_{ln} + g_{ml} A_{k_i\ n}^{\ l} = 0 \tag{S27}$$

This relation is important for us to predict the emergence of ELs and NIPs. More details can be found in [10].

The local metric g is important for us to understand the evolution of eigenstates. In a specific region, g is invariant. For example in *PT*-exact phases, the local metrics in Region I and Region III are in the following forms

$$g_{\mathrm{I}} = \begin{bmatrix} 1 & 0 \\ 0 & -1 \end{bmatrix},\ g_{\mathrm{III}} = \begin{bmatrix} -1 & 0 \\ 0 & 1 \end{bmatrix} \tag{S28}$$

Here the sequence of eigenvalues is defined by sorting the corresponding eigenvalues from small to large. The geometric phase is an integration of the affine connection

$$U^{-1} = \mathrm{P}\exp\left(\int_{\mathbf{k}(0)}^{\mathbf{k}(\xi)} d\mathbf{k} A_{\mathbf{k}}\right) \tag{S29}$$

where P is the path ordering operator because the affine connection is a matrix. It is not difficult to find out that the two eigenstates experience Lorentz boost and the geometric phase is simply

$$U^{-1} = \exp\gamma T \tag{S30}$$

where T is the Lie algebraic generator of SO(1,1) group

$$T=\begin{bmatrix}0 & 1\\ 1 & 0\end{bmatrix} \tag{S31}$$

and can be derived from Eq. (S27). Next, we define the path parameter θ (see Fig. S3a), with $f_3=\cos\theta$ and $f_2=\sin\theta$. The evolution of eigenvalues and eigenstates along the path α ($-\pi/4\le\theta\le\pi/4$) is shown in Fig. S3b1 and b2, respectively. Note that the eigenstates have been rescaled. As can be indicated in Fig. S3b2, the two eigenstates are rotating in opposite directions, and resultantly, they evolve from parallel states to antiparallel states, which is typical for frame deformations. This process occurs because γ varies from $+\infty$ to 0 and to $-\infty$, and the infinity of γ is provided by the ELs, i.e. the path departs from EL_1 and terminates at EL_2. It is thus understandable that the frame deformation is a result of hyperbolic transformation, i.e. the Lorentz boost in general relativity [8]. In Region III, the evolution of eigenstates is similar to that in Region I, simply the two eigenstates swap.

In broken phases, the local metrics are both

$$g_{\mathrm{II,IV}}=\begin{bmatrix}0 & 1\\ 1 & 0\end{bmatrix}, \tag{S32}$$

and the evolution of eigenstates is still defined on SO(1,1) group. The difference is that the two eigenstates become complex conjugate, and the frame deformation process is extended to the complex space. Results for path β ($\pi/4\le\theta\le3\pi/4$) is provided in Fig. S3c. As shown in Fig. S3c2-c3, the initially parallel eigenstates bifurcate to form a conjugate pair, and finally evolve to two anti-parallel imaginary vectors.

With the above frame deformation process on any of the paths aforementioned, one can already determine that an NIP can be formed by the intersection of the two ELs (or ESs). Hence, an open path joining ELs (or ESs) can provide a lot of information on the intersection NIP (or NIL) of the ELs (or ESs). This is essentially different from isolated singularities, for which a path is only meaningful whenever it is closed. Therefore, if we consider a closed loop circulating a hypersurface singularity that is partitioned into several paths by the ELs (or ESs), it is necessary to investigate each open path that terminates at the ELs (or ESs) and then discuss their combinations. Our former work [10] has established the relation between the frame deformation with the conventional Berry phase, which is also mentioned in the main text to explain the topologically protected edge states.

4. Some other nontrivial loops and typical trivial loops in parameter space

In Fig. 2 of the main text, we introduced some typical nontrivial loops and the corresponding topological invariants. Since the number of elements in the group (Eq. 4) is infinitely large, and some elements other than Fig. 2 are also useful, here we give a brief introduction on these invariants and the corresponding path combinations in parameter space. Some typical paths (or loops) carrying trivial topological invariants will also be introduced.

Figure S4(a) shows the path product $\alpha'\beta$. Note that the basepoint has been fixed at A (or A'), and thus we cannot exchange the order in the product (i.e. $\beta\alpha'$). Exchanging the order in the product means that the basepoint is changed from A (or A') to B (or B'). In homotopy theory, one will obtain another fundamental group by changing the basepoint without changing the order parameter space, and the groups obtained by changing the basepoint are isomorphic to each other since the quotient space M is path-connected. It is not difficult to find out that $\alpha'\beta=\alpha'\alpha^{-1}\alpha\beta$, and thus the corresponding topological

invariant is $Z_2^{-1}Z_1$, which is an element of the group (Eq. 4). The path combination $\beta'^{-1}\beta$ is totally in broken phases, and is a counterpart of Fig. 2(b). Since $\beta'^{-1}\beta$ can be obtained as the path product $\beta'^{-1}\alpha'^{-1}\alpha'\alpha^{-1}\alpha\beta$, it is thus obtained that the invariant on the loop is $Z_3^{-1}Z_2Z_1$. In a similar way, the path combination in Fig. S4(c) $\alpha\beta'$ can be obtained as the product $\alpha\alpha'^{-1}\alpha'\beta'$, and the invariant on the loop is simply $Z_2^{-1}Z_3$.

Typical loops carrying trivial topological invariant are shown in Fig. S4(d-f). The loop l does not touch any EL, and thus is confined in only one region, which is always trivial because it cannot enclose any singularity. As we move the loop across the EL, l is decomposed into two paths l_1 and l_2 [Fig. S4(e)]. As the terminal points of l_1 (or l_2) can be identified, l_1 (or l_2) is also a loop in quotient space M, but is a trivial loop that can shrink to a point. Therefore, the combination l_1l_2 is also trivial. By stretching the loop to cross the other EL [see Fig. S4(f)], l becomes a composite of $l_1l_3l_4l_5$. Since both l_1 and l_4 correspond to trivial loops in quotient space M, the composite is equivalent to the combination l_3l_5. In addition, paths l_3 and l_5 are along opposite directions and are homotopic to α^{-1} and α, respectively. It is thus not difficult to find out that the combination $l_1l_3l_4l_5$ remains trivial. *From this analysis, we can conclude that a loop (or a path) encountering ELs through continuous deformations will not change the topology. In contrast, encountering NIPs is not allowed, which will change the topology.* Similar discussion can also be found in [10].

5. Non-reciprocal tight binding model realizing chain of NILs

Apart from the continuous model in the main text, the chain of NILs can also be realized with a periodic system with non-reciprocal hoppings. Here we consider a 3D fcc lattice model in Fig. S5a, and the corresponding Brillouin zone is shown in Fig. S5b, where M and N denote two inequivalent lattice sites with opposite onsite energies $\pm E_0$, respectively. The hopping between M and N (on dark green bonds) is non-reciprocal ($M\rightarrow N$: t_1, $M\rightarrow N$: $-t_1$), and the hoppings on yellow and red bonds [between the adjacent sites in the same sublattice but in different directions, i.e. yellow bonds: $\vec{r}_M \rightarrow \vec{r}_M + \vec{a} + \vec{b}$ and $\vec{r}_N \rightarrow \vec{r}_N + \vec{a} - \vec{b}$; red bonds: $\vec{r}_M \rightarrow \vec{r}_M + \vec{a} - \vec{b}$ and $\vec{r}_N \rightarrow \vec{r}_N + \vec{a} + \vec{b}$] are characterized by t_2 and $-t_2$, respectively. The corresponding real space Hamiltonian is given by

$$\begin{aligned} H_r = & \sum_{\substack{\vec{r}_M \in \vec{G}_M \\ \vec{\alpha}=\vec{a},\vec{b},\vec{c}}} t_1(a^\dagger_{M,\vec{r}_M} a_{N,\vec{r}_M+\vec{\alpha}} + a^\dagger_{M,\vec{r}_M} a_{N,\vec{r}_M-\vec{\alpha}}) - h.c. + E_0(a^\dagger_{M,\vec{r}_M} a_{M,\vec{r}_M} - a^\dagger_{N,\vec{r}_N} a_{N,\vec{r}_N}) \\ & + \sum_{\substack{\vec{r}_h \in \vec{G}_h \\ h=M,N}} \mathrm{sgn}(h) t_2(a^\dagger_{h,\vec{r}_h} a_{h,\vec{r}_h+\vec{a}+\vec{b}} + h.c. - a^\dagger_{h,\vec{r}_h} a_{h,\vec{r}_h+\vec{a}-\vec{b}} - h.c.) \end{aligned} \tag{S33}$$

where $\vec{a}$, $\vec{b}$ and $\vec{c}$ are the set of orthogonal lattice vectors connecting lattice sites M and N (see Fig. S5a). Here sgn(h)=1 and –1 for $h=M$ and N, respectively. The corresponding **k**-space Hamiltonian can be obtained by Fourier transformation

$$\begin{aligned} H_k = & t_1(e^{ik_x} + e^{-ik_x} + e^{ik_y} + e^{-ik_y} + e^{ik_z} + e^{-ik_z}) a^\dagger_{M,k} a_{N,k} - h.c. \\ & + E_0(a^\dagger_{M,k} a_{M,k} - a^\dagger_{N,k} a_{N,k}) \\ & + t_2(e^{ik_x+ik_y} + e^{-ik_x-ik_y} - e^{ik_x-ik_y} - e^{-ik_x+ik_y})(a^\dagger_{M,k} a_{M,k} - a^\dagger_{N,k} a_{N,k}) \end{aligned} \tag{S34}$$

and the **k**-dependent Hamiltonian can be expressed as

$$H_1(\mathbf{k})=\begin{bmatrix} E_0+2\sin k_x \sin k_y & \cos k_x+\cos k_y+\cos k_z \\ -\cos k_x-\cos k_y-\cos k_z & -E_0-2\sin k_x \sin k_y \end{bmatrix} \tag{S35}$$

It is can be observed that $f_3(\mathbf{k})=E_0+2\sin k_x \sin k_y$ and $f_2(\mathbf{k})=\cos k_x+\cos k_y+\cos k_z$, and thus the Hamiltonian preserves the symmetries in Eq. (1). If E_0=0, the onsite energies on *M* and *N* are the same, and the system has mirror symmetries in the *x* and *y* directions. Resultantly, the band structure is symmetric about $k_x=\pi/d_L$ and k_y=0 planes. The ESs and NILs for E_0=0 are plotted in Fig. S5c, where the red and green surfaces are ESs satisfying $f_2=\mp f_3$, respectively. As can be seen, a chain of NILs is formed on the intersection line of the mirror planes ($k_x=\pi/d_L$ and k_y=0, see Fig. S5c). The orange dashed loop (Fig. S5d) is a combination $(\alpha'\beta'\alpha\beta)^2$ that carries a squared topological invariant $(Z_3Z_1)^2$, which means that the enclosed NILs cannot annihilate each other. The blue dashed loop does not traverse any ES and is trivial. The two loops set necessary condition for the presence of the chain of NILs. Apart from the topological invariants, the mirror symmetries is also an important factor to the emergence of chain of NILs, because the chain points are on the intersection line (red arrows) of the two mirror planes ($k_x=\pi/d_L$ and k_y=0). A nonzero E_0 can break the mirror symmetries in k_x and k_y directions, which eliminates the intersection points (as shown in Fig. S5e). However, the breaking of mirror symmetries does not affect the topology on the loops. As shown in Fig. S5e, the blue loop is still trivial, because it does not touch any ESs. The topological invariant on the orange loop is conserved [still $(Z_3Z_1)^2$], as the traversed ESs remain the same (Fig. S5d and S5f). Therefore, the emergence of the chain of NILs not only requires the symmetries in Eq. (1), but also needs two mirror symmetric planes. Such a structure is not stable against perturbations to the Hamiltonian, deforming the Hamiltonian without changing the symmetries can easily eliminate the chain of NILs as shown in Fig. 3 of the main text.

References:

[1] A. Mostafazadeh, Pseudo-Hermitian representation of quantum mechanics, Int. J. Geo. Meth. Mod. Phys. **7**, 1191-1306 (2010).

[2] R. Zhang, H. Qin, J. Xiao, PT-symmetry entails pseudo-Hermiticity regardless of diagonalizability, J. Math. Phys. **61**, 012101 (2020).

[3] A. Mostafazadeh, Pseudo-Hermiticity versus PT-symmetry III: Equivalence of pseudo-Hermiticity and the presence of antilinear symmetries, J. Math. Phys. **43**, 3944-3951 (2002).

[4] Ş. K. Özdemir, S. Rotter, F. Nori, et al. Parity–time symmetry and exceptional points in photonics[J]. Nat. Materials **18**, 783-798 (2019).

[5] E. H. Spanier, Algebraic topology, Springer Science & Business Media, 1989.

[6] P. Gajer, The intersection Dold-Thom theorem, Topology **35**, 939-967 (1996).

[7] W. Ebeling, The monodromy groups of isolated singularities of complete intersections, Springer, 2006.

[8] D. Z. Freedman, A. Van Proeyen, Supergravity, Cambridge university press, 2012.

[9] T. Frankel, The geometry of physics: an introduction, Cambridge university press, 2011.

[10] J. Hu, R. Y. Zhang et al. Non-Hermitian swallowtail catastrophe revealing transitions across diverse topological singularities, Research Square preprint [https://doi.org/10.21203/rs.3.rs-1853770/v1] (2022).

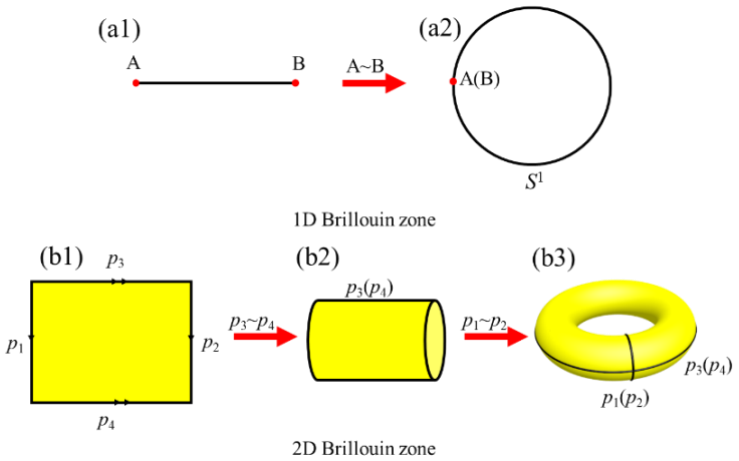

Fig. S1. Quotient space of momentum space in periodic systems. (a1)-(a2) The quotient space of 1D Brillouin zone is a circle (S^1) by identifying the two points on the Brillouin zone boundary. (b1)-(b3) Construction of quotient space of 2D Brillouin zone. Identifying the boundaries p_3 with p_4 gives a cylinder, which becomes a torus by identifying p_1 with p_2.

$$V := \mathbb{R}^2$$

$$S := \{\mathbb{R}^2, > \{|\, f_2 \,| = |\, f_3 \,|\}, > \{f_2 = f_3 = 0\}\}$$

$T_1 :=$ $\mathbb{R}^2$

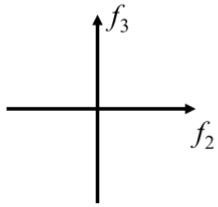

$T_2 :=$

$T_3 :=$

Fig. S2. Stratified space of the 2D plane with ELs and NIP.

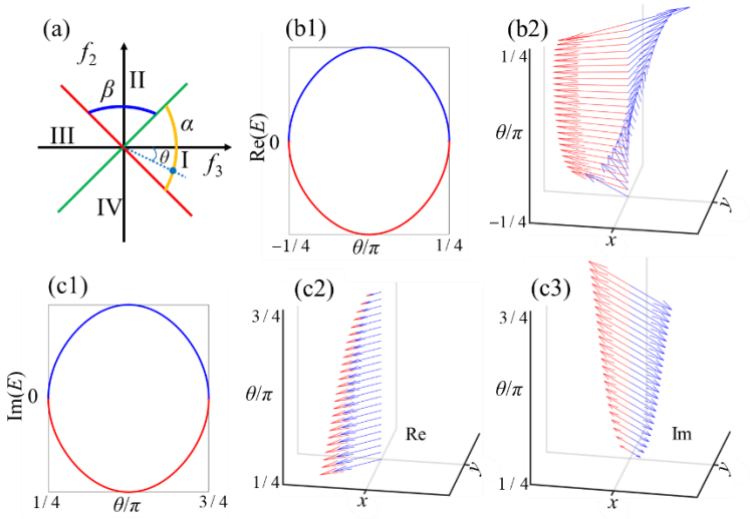

Fig. S3. Frame deformation along different paths. (a) Paths α and β in parameter space. θ denotes the path parameter, i.e. $f_3=\cos\theta$, $f_2=\sin\theta$, $-\pi/4\le\theta\le\pi/4$ for α, $\pi/4\le\theta\le3\pi/4$ for β. (b1-b2) Evolution of eigenvalues (real part, b1) and eigenstates along path α. (c1-c3) Evolution of eigenvalues (imaginary part, c1) and eigenstates (c2, real part; c3, imaginary part) along path β.

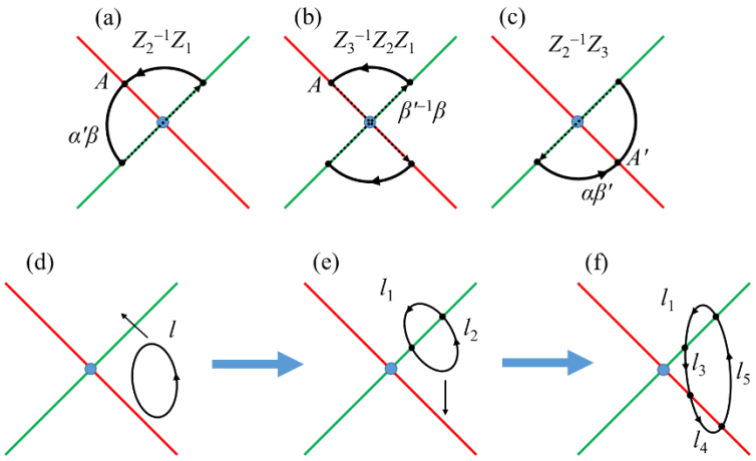

Fig. S4. (a-c) Some other nontrivial loops and the corresponding topological invariants (other than Fig. 2) taking from the group Eq. 4. (d) A loop without touching ELs is confined within a specific region and is trivial. (e) Moving the loop along the black arrow direction [see (d)], the loop becomes a composite of paths l_1 and l_2. Both of l_1 and l_2 are trivial, and their composite loop is also trivial. (f) Stretching the loop along the black arrow direction in (e), the loop crosses EL_1 and becomes a composite of paths $l_1l_3l_4l_5$. The path l_4 corresponds to a trivial loop in quotient space M. The paths l_5 and l_3 are in opposite directions, and are homotopic to α and α^{-1}, respectively. The path product $l_1l_3l_4l_5$ is thus trivial.

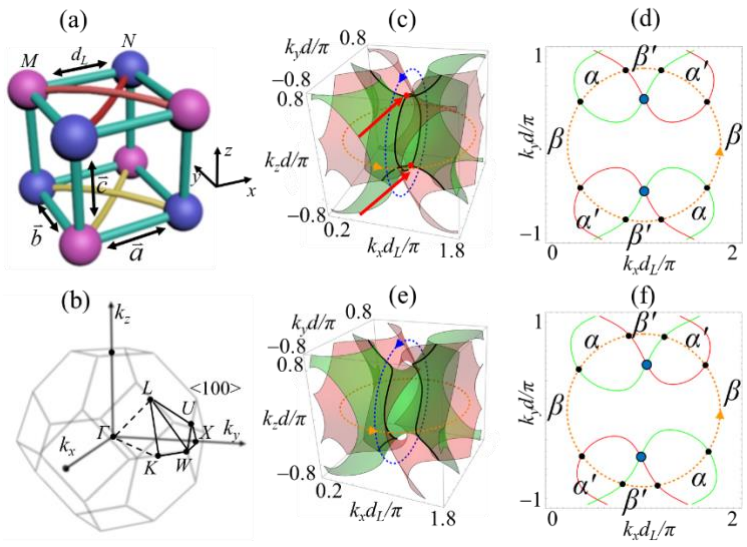

Fig. S5. Proposal of an fcc lattice model to realize the chain of NILs. (a) fcc lattice with two sites *M* (blue balls) and *N* (pink balls). The interspace distance between *M* and *N* is d_L, and $\vec{a}$, $\vec{b}$ and $\vec{c}$ are bond vectors. The hopping on dark green bonds is non-reciprocal (*M*→*N*: t_1, *N*→*M*: $-t_1$). The hopping on the same lattice sites in different directions (in $\vec{a}+\vec{b}$ and $\vec{a}-\vec{b}$) have opposite signs (hopping on yellow bonds: t_2, hopping on red bonds: $-t_2$). (b) First Brillouin zone of the fcc lattice. (c, e) ESs (red and green surfaces) and NILs (black lines) for $E_0=0$ and $E_0\neq 0$ in Eq. (6). (c) has a chain of NILs, which is symmetric with respect to <100> plane. The intersecting points on the chain are labelled with red arrows. (d, f) Cross section of the plane $k_z=0$ (where the orange loop locates) for (c) and (d), respectively. The topological charge on the loop is conserved even though the mirror symmetries are broken.